The linearity and chemical bond of UO_2^{2+} revisited: a comparison study with UN_2 and UE_2^{2+} (E = S, Se, Te) based on relativistic calculations

Ayaki Sunaga,* Chihiro Tabata, and Tomoo Yamamura

Institute for Integrated Radiation and Nuclear Science, Kyoto University, Osaka 590-0494, Japan

E-mail: sunaga.ayaki.5x@kyoto-u.ac.jp

Phone: +81 072 451 2642

Abstract

The stability and electronic structure of UO_2^{2+} are compared with those of UN_2 and UE_2^{2+} (E = S, Se, Te) based on four- and two-component relativistic Hamiltonians. We observed that the Hartree-Fock method overestimates the stability of the linear structures of UO_2^{2+} and UN_2. In addition to the conventional mechanism based on valence orbitals, we proposed another mechanism that the small energy difference between U's $6p_{3/2}$ and O's $\sigma(2s)$ orbitals destabilizes the bent structure of UO_2^{2+}. The validity of the analysis based on the DFT method was evaluated using coupled-cluster method. The slightly bent structures of UO_2^{2+} and UN_2 are feasible from the viewpoint of energetic stability: the destabilized energy at 160 degrees is 0.144 eV and 0.059 eV for UO_2^{2+} and UN_2, respectively. The U-X bond (X = N,O) is rigid in the slightly bent structure, and it corresponds to the conservation of the feature of the chemical

bond. For UE_2^{2+}, core-valence orbitals mainly affect the stability of these molecules, including UO_2^{2+} and UN_2. In UE_2^{2+}, the $6p$ hole is fairly modest, and the $6p$ hole in UO_2^{2+} is a unique feature in uranium-chalcogen systems.

INTRODUCTION

The improvements in both experimental and theoretical techniques provide new glimpses into of the electronic structure of actinides complexes. The multiple bonds of Uranium-ligands molecules are observed based on the multireference correlation methods.[1–5] The geometrical and electronic structures of the complexes, including uranium-metal bonds, are reported from both experimental and theoretical viewpoints.[6–9] The chemical bonds of actinide dimer have been investigated,[10,11] but the correct inclusion of the spin-orbit effect changes the bond order of U_2 dimer from a quintuple bond[12] to a quadruple bond.[13]

In contrast to the aforementioned recent studies, the uranyl dication UO_2^{2+} has been studied extensively.[14–17] It is the fundamental structure of uranium complexes, as the first uranium compounds studied using X-ray crystallography (sodium uranyl acetate) contain a uranyl ion.[18,19] The contribution from U's $5f$ orbital to chemical bonds has been studied since the 1950s.[20–22] Einstein and Pryce formulated a model of the chemical bonds of UO_2^{2+} to explain their magnetic properties.[23] They assumed that σ-type orbitals can be formed, but π-type orbitals are strongly localized to the oxygen atoms. The initial semi-empirical[24–28] and *ab initio*[29,30] calculations about the electronic structure of UO_2^{2+} were reported around 1980. Spectroscopic constants and excitation energies have also been investigated in detail, based on relativistic correlated methods.[31–35]

The linearity of UO_2^{2+} has been confirmed since the 1970s from some studies on its vibrational mode in experiments.[36–39] From the theoretical perspective, various models have been suggested to explain linearity. At the Huckel level, it is observed that $5f$ and $6d$ orbitals in UO_2^{2+} prefer the bent structure. When the $6p$ orbital is included in the calculation, the linear structure gains stability, while the $6p$ orbital causes UO_2^{2+} to bend.[26] The direct

contribution of U($6p$)π-O($2p\pi$) anti-bonding,[40] the lack of U($5f$)π-O($2p\pi$) bonding,[28] and the balance between $5f$ and $6d$ orbitals in the hybridization[30,41] are also suggested. Along with the bent structure, the triangle-type and U-O-O-type structures are also unstable.[42] Calculations using the correlation method[31–35] or density functional theory (DFT)[34,35,43–46] levels have yielded the UO_2^{2+} equilibrium structure (i.e., linear structure) and associated vibrational frequencies.[47–49]

The linearity of UO_2^{2+} has been already explained, but it should be noted that there exist two methods to synthesize molecules containing a bent cis-dioxido UO_2^{2+},[50,51] which should be unstable based on the aforementioned theoretical studies. Meanwhile, the molecule reported in ref. 50 was under investigation, and the reproduction of its synthesis was not successful.[52] Although the UO_2^{2+} in a complex becomes bent via physical pressure,[53] complexes consisting of a slightly bent UO_2^{2+} structure are observed even without physical pressure.[54–56] The maximum bent angle in Table 1 of ref. 54 is about 20 degrees.

In this study, the stability of the UO_2^{2+} is analyzed based on the four-component relativistic calculations, by comparing it UN_2 and UE_2^{2+} (E = S, Se, Te). We observed that the Hartree-Fock (HF) method, which has been employed for linearity for long time in previous works, overestimates the instability of UO_2^{2+} at bent structures. The accuracy of the DFT is evaluated using the coupled-cluster singles and doubles with approximate triples correction (CCSD(T)) method. The analysis based on the Khon-Sham (KS) orbital suggests a new mechanism for the stabilization of the linear structure: the small gap between U's $6p_{3/2}$ and O's $2s$ destabilizes the bent structure of UO_2^{2+} significantly, as compared to that in UN_2. This stabilization mechanism is not found in UE_2^{2+} because of the destabilized ns orbital of the E atom, where n is the principal quantum number. It is found that the U-X bond of UO_2^{2+} and UN_2 are rigid with respect to the bending of the structure, based on the optimized bond length and the chemical bond.

COMPUTATIONAL DETAILS

Methods

For all calculations, the development versions (418ce89 and 4596ff6) of the DIRAC code[57,58] were used. All basis sets were employed in their uncontracted forms and their small components were generated by the restricted kinetic balance.[59] The Gaussian-type nuclear charge model[60] is used for all nuclei in the calculation. The chemical bonds are analyzed by the projection analysis based on the canonical and localized orbitals.[61]

For UO_2^{2+} and UN_2, the HF, DFT, and CCSD(T)[62] methods were employed for the calculations of electronic structures. The Dirac-Coulomb-Gaunt Hamiltonian was employed at the Hartree-Fock and the PBE0[63,64] levels. The exact two-component molecular mean-field approximation (X2Cmmf)[65] to the Dirac-Coulomb-Gaunt Hamiltonian (^{2}DCG^M) was employed for the CCSD(T) level. In this approach, the four-component calculation including the Gaunt term is done at the SCF level, and the two-component calculation is done at the correlation level. In the CCSD(T) calculation, 34 electrons beyond the $5d$ orbitals of the uranium atom, and the $2s$ and $2p$ electrons of the oxygen and nitrogen atoms are correlated. The virtual space is truncated at approximately 10 E_H. The two-electron integrals between small components (SS|SS) are explicitly taken into account and the dyall.cv3z basis sets[66,67] are employed.

For UE_2^{2+}, the DCG Hamiltonian and PBE0 DFT functional were employed for all calculations. The two-electron integrals between small components (SS|SS) are replaced with classical coulombic interaction[68] and the dyall.3zp basis sets[66,67] are employed.

Chemical bond analysis

To analyze the electronic structure of the target molecules, we employed the projection analysis.[61] In previous works on UO_2^{2+}, the Mulliken population analysis[69] was often employed,[31,41,43] but its basis set dependence[70] may give unreliable results. In the projection

analysis, the process is same as that in the Mulliken population analysis, but the basis set dependence is avoided by expanding the molecular orbital in terms of the atomic orbitals[61]

$$|\psi_i\rangle = \sum_{Ap} \left|\psi_p^A\right\rangle c_{pi}^A + \left|\psi_i^{\mathrm{pol}}\right\rangle. \tag{1}$$

Here, i, p, and A are the indices of the molecular orbital, atomic orbital, and the nucleus in the molecule, respectively. c is the coefficient of expansion. The polarization contribution $\left|\psi_i^{\mathrm{pol}}\right\rangle$ is the orthogonal complement that is not spanned by the atomic reference orbitals. We removed this contribution using the intrinsic atomic orbital scheme of Knizia.[71] In this study, gross population is employed to provide the population of the atomic orbitals. The gross population N of each atomic orbital p in the molecular orbital i is defined as follows:

$$N_{ip}^A = \left(c_{pi}^A\right)^2 + \sum_{p>q,AB} c_{pi}^A c_{qi}^B S_{pq}^{AB}, \tag{2}$$

where S_{pq}^{AB} is the overlap between ψ_p^A and ψ_q^B. We employed two kinds of molecular orbitals. The first is the canonical molecular orbital (CMO), which is the eigenfunction of the Fock operator. In the KS DFT framework, the eigenvalue of each CMO corresponds to the ionization energy in Janak's theorem.[72] However, since it is widely distributed in the entire molecule, it does not provide the information about chemical bonds. The second is the localized molecular orbital (LMO). It spans a minimum of atomic centers, and distinguishes bonding or non-bonding-type orbitals. When only one atom contributes to the LMO, it results in a non-bonding-type orbitals and vice-versa. In this study, Pipek-Mezey scheme[73] was used for the localization. The CMO and LMO can be transformed into each other by using unitary transformation.

We employed the following bond order:[74]

$$\text{Bond order} = \frac{N_{\text{bonding}} - N_{\text{antibonding}}}{2} \tag{3}$$

Here, N_{bonding} and $N_{\mathrm{antibonding}}$ are the number of electrons in the bonding-type and antibonding-type orbitals, respectively. The LMOs can be separated into core, lone-pair, and bonding-type LMOs. In this definition, the number of electrons in the antibonding-type orbital ($N_{\mathrm{antibonding}}$) is always zero.

The atomic reference orbitals are generated with the fractional occupation method with the PBE0 functional. The electronic configurations are as follows: [He]$2s^2 2p^3$ for N, [He]$2s^2 2p^4$ for O, [Ne]$3s^2 3p^4$ for S, [Ar]$4s^2 4p^4$ for Se, [Kr]$5s^2 5p^4$ for Te, and [Rn]$5f^3 7s^2 6d^1$ for U atoms, respectively. One may think the dication of the uranium atom whose electronic ground state is [Rn]$5f^4$ [75] should be employed as the reference of the atomic orbital, but we use the neutral one to estimate the contribution from the $6d$ and $7s$ orbitals.

RESULTS AND DISCUSSION

If not explicitly stated otherwise, the U-X (X = N, O) bond lengths in UO_2^{+2} and UN_2 are fixed to 1.704 Å and 1.736 Å, respectively, which were optimized using the ECP60MDF and CCSD(T) methods.[46] The bond lengths of US_2^{2+}, USe_2^{2+}, and UTe_2^{2+} are 2.190 Å, 2.358 Å 2.680 Å, which were optimized at the linear structure with the DCG-PBE0 method in this work. The molecules studied in this work are presented in Figure 1. First, the largely bent structures of UO_2^{+2} and UN_2 are shown to display the trend explicitly. Next, slightly bent structures that are experimentally observed are discussed as practical cases. The chemical bonds based on the localized orbital are also analyzed. Finally, the comparison between UO_2^{+2} and UE_2^{+2} (E = S, Se, Te) are discussed. In the figures, ω is the projection quantum number of the total electronic angular momentum, j, along the molecular axis.

Largely bent structures

The linearity of UO_2^{2+} is investigated using the HF[41] or semi-empirical method,[26,28] but the low accuracies of these methods are non-negligible. The HF method can reproduce the

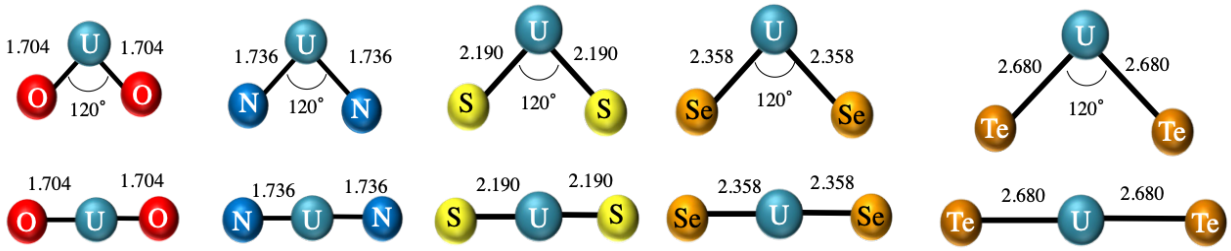

Figure 1: Structures of the studied molecules at 120 and 180 (linear) degrees. The bond lengths are optimized in the linear structure.

stability of the linear structure, but it overestimates the instability of the bent structure (Figure 2). The destabilization energies of UO_2^{2+} at the HF, PBE0, and CCSD(T) levels are 1.79 eV, 1.11 eV and 1.12 eV at 120 degrees, respectively. Meanwhile, the values at the PBE0 level reasonably agree with those at the CCSD(T) level for both UO_2^{2+} and UN_2.

The HF method cannot predict the degree of the instabilities of UO_2^{2+} and an isoelectronic system, UN_2, at the orbital energy level (Figure 3). The bent structure of UO_2^{2+} is more unstable than that of UN_2 at the CCSD(T) level (Figure 2), while according to the sum of the HF orbital energies, the bent structure of UO_2^{2+} is more stable than that of UN_2. The choice of "valence orbitals" is essential for an energetical analysis based on the orbital energies. We employed the following two models: i) 8orb., wherein HOMO to HOMO-7 were taken into account, and ii) 10orb., wherein HOMO to HOMO-9 were taken into account. At the PBE0 level, the 8orb. model reproduces the trend of CCSD(T), while the 10orb. model cannot predict the linearity of UO_2^{2+} and UN_2 (Figure 4). We employ the 8orb. model in our later analyses. The full MO diagrams of UO_2^{2+} and UN_2, used to discuss their stabilities, are shown in Figure 5 and 6.

There are two ways of taking the important contributions in the 8orb. model. Although the conventional analysis is based on a few valence orbitals[26,28,40,41] even at the DFT level, we suggest a new mechanism based on the U's $6p_{3/2}$ and O and N's $2s_{1/2}$ orbitals. In Table 1, the energy contribution from the KS orbital to the destabilized energy at 120 degrees is shown and compared with the CCSD(T) destabilized energy. Both models hold good for

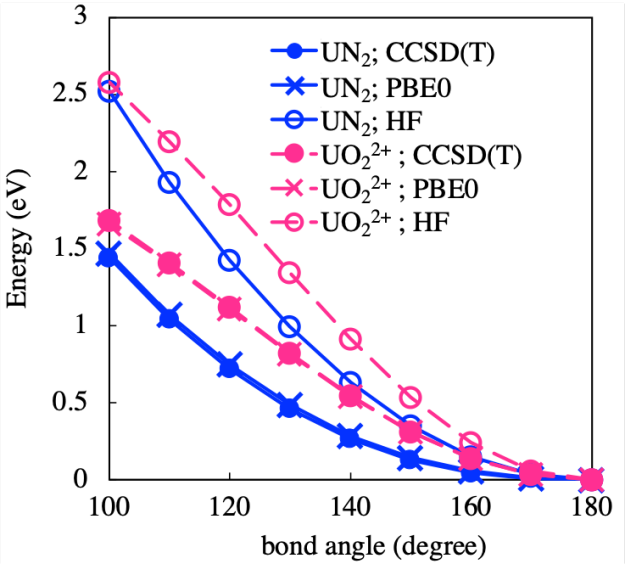

Figure 2: The destabilization of the total energies in the linear structures of UN_2 and UO_2^{2+} at the CCSD(T), PBE0, and HF levels as a function of angle (from 180 to 100 degrees). The U-X (X = N, O) bond lengths are fixed: 1.736 Å and 1.704 Å for UN_2 and UO_2^{2+}, respectively.

UO_2^{2+}, whereas for UN_2, the values of the "HOMO - HOMO−2" model qualitatively agree with the CCSD(T) values, but the "HOMO−6 - HOMO−7" model shows better agreement with the CCSD(T) values. The HOMO−6 and HOMO−7 capture the dominant effect that determines the molecular structure.

Table 1: Comparison of destabilized energies (eV) at 120 degrees and 180 degrees for UO_2^{2+} and UN_2 at the CCSD(T) and PBE0 levels. "n-m" refers to the sum of the orbital energies from the n^{th} to m^{th} KS orbitals at the PBE0 level.

	UO_2^{2+}	UN_2
CCSD(T)	1.12	0.72
HOMO - HOMO − 7	1.16	0.77
HOMO - HOMO − 2	1.11	0.49
HOMO − 6 - HOMO − 7	1.21	0.73

For "HOMO - HOMO−2", a similar trend is observed in UO_2^{2+} and UN_2 (Figure 7). HOMO ($\sigma_{u,1/2}$) and HOMO-1 ($\sigma_{g,1/2}$) contribute to the destabilization of the bent structure. At 120 degrees, the contribution of $5f_{7/2}$ is decreased by 20 percent in HOMO whereas the $5f$ population is increased in HOMO−1 in UO_2^{2+} and UN_2. Some previous studies

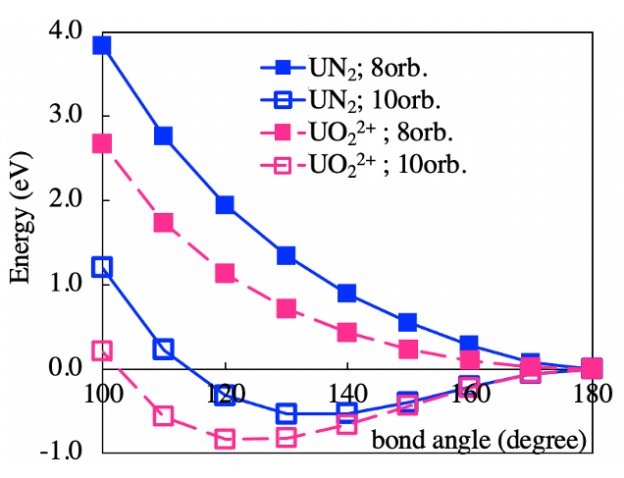

Figure 3: The destabilization of the sum of HF orbital energies in the linear structures of UN_2 and UO_2^{2+} as a function of angle (from 180 to 100 degrees). The U-X (X = N, O) bond lengths are fixed: 1.736 Å and 1.704 Å for UN_2 and UO_2^{2+}, respectively.

based on the semi-empirical method[28,40] and the HF method with a relativistic effective core potential[30] tried to attribute the linearity to the π-bonding ($5f\pi$-$2p\pi$ or $6p\pi$-$2p\pi$). However, the sophisticated calculations in our study show that the $5f$-$2p$-dominant σ_u and $2p$-dominant σ_g contribute to the stability of the linear structure (Table 2 and Figure 7). For UN_2, the contributions of $7s$ and $6d$ are larger than those in UO_2^{2+} (Figure 7 and Table 2). This is because the molecular orbital energies of the neutral UN_2 are higher, and energetically closer to the $7s$ and $6d$ of uranium than the cationic UO_2^{2+}.

Table 2: Projection analysis of the three highest canonical KS orbitals of UO_2^{2+} (R = 1.704 Å) and UN_2 (R = 1.736 Å). The KS orbital energies (ε) are also shown. X refers to O or N atoms.

	mol.	angle	ε (eV)	U6p$_{3/2}$	U5f$_{5/2}$	U5f$_{7/2}$	U6d$_{3/2}$	U6d$_{5/2}$	U7s$_{1/2}$	X2s$_{1/2}$	X2p$_{1/2}$	X2p$_{3/2}$
HOMO	UO_2^{2+}	180	−23.71	0.07	0.14	0.43	0.00	0.00	0.00	0.01	0.24	0.09
		120	−23.18	0.08	0.10	0.25	0.01	0.05	0.00	0.01	0.31	0.19
	UN_2	180	−6.73	0.05	0.14	0.51	0.00	0.00	0.00	0.01	0.23	0.06
		120	−6.34	0.04	0.12	0.30	0.01	0.08	0.00	0.02	0.26	0.16
HOMO-1	UO_2^{2+}	180	−24.42	0.00	0.00	0.00	0.01	0.03	0.02	0.07	0.37	0.48
		120	−23.90	0.03	0.11	0.14	0.03	0.04	0.00	0.01	0.12	0.51
	UN_2	180	−7.09	0.00	0.00	0.00	0.02	0.05	0.13	0.05	0.32	0.42
		120	−6.90	0.02	0.16	0.17	0.04	0.08	0.01	0.02	0.13	0.36
HOMO-2	UO_2^{2+}	180	−24.67	0.02	0.12	0.23	0.00	0.00	0.00	0.00	0.00	0.63
		120	−24.60	0.00	0.16	0.06	0.04	0.02	0.00	0.01	0.18	0.53
	UN_2	180	−7.48	0.01	0.15	0.26	0.00	0.00	0.00	0.00	0.00	0.57
		120	−7.55	0.00	0.18	0.07	0.07	0.05	0.00	0.01	0.11	0.50

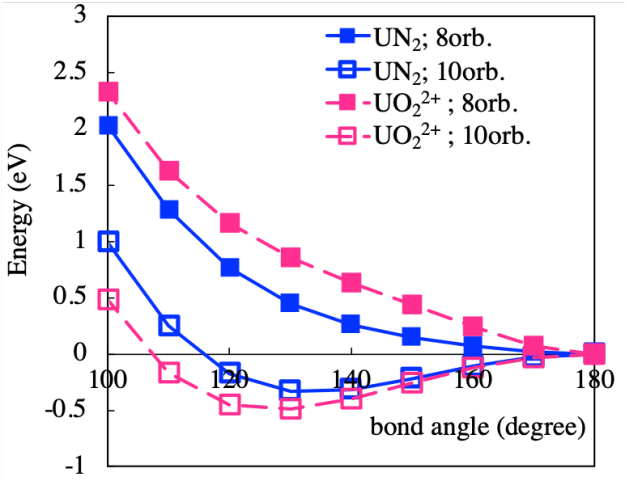

Figure 4: The destabilization of the sum of KS orbital energies in the linear structures of UN_2 and UO_2^{2+} as a function of angle (from 180 to 100 degrees). The U-X (X = N, O) bond lengths are fixed: 1.736 Å and 1.704 Å for UN_2 and UO_2^{2+}.

Moreover, a significant difference is observed in "HOMO−6 - HOMO−7" for UO_2^{2+} and UN_2 (Figure 8). In the linear structure, the HOMO−7 of UO_2^{2+} mainly consists of U's $6p_{3/2}$ while that of UN_2 mainly consists of N's $2s_{1/2}$. This is because O's $2s_{1/2}$ is energetically more stable than N's $2s_{1/2}$. For the neutral atom at the DCG-PBE0 level, the orbital energies of N's $2s_{1/2}$, U's $6p_{3/2}$, and O's $2s_{1/2}$ are −21.2 eV, −23.1 eV, and −27.1 eV, respectively. In the UO_2^{2+} molecule, the $2s_{1/2}$-dominant orbital with bonding-type character (HOMO−8) is energetically closer to the HOMO−7. This results in a strong anti-bonding type mixing

Table 3: Projection analysis of HOMO-6, HOMO-7 and HOMO-8 of canonical KS orbitals of UO_2^{2+} (R = 1.704 Å) and UN_2 (R = 1.736 Å). The KS orbital energies (ε) are also shown. X refers to O or N atoms.

	mol.	angle	ε (eV)	U6$s_{1/2}$	U6$p_{1/2}$	U6$p_{3/2}$	U5$f_{5/2}$	U5$f_{7/2}$	U6$d_{3/2}$	U6$d_{5/2}$	U7$s_{1/2}$	X2$s_{1/2}$	X2$p_{1/2}$	X2$p_{3/2}$
HOMO-6	UO_2^{2+}	180	−32.54	0.00	0.02	0.31	0.00	0.02	0.02	0.00	0.00	0.51	0.08	0.06
		120	−33.59	0.00	0.01	0.40	0.00	0.01	0.00	0.02	0.02	0.46	0.05	0.03
	UN_2	180	−13.56	0.00	0.02	0.15	0.00	0.03	0.03	0.00	0.00	0.65	0.07	0.05
		120	−14.78	0.00	0.01	0.20	0.00	0.01	0.01	0.06	0.05	0.60	0.03	0.02
HOMO-7	UO_2^{2+}	180	−38.64	0.00	0.03	0.97	0.00	0.00	0.00	0.00	0.00	0.00	0.00	0.00
		120	−36.38	0.01	0.02	0.51	0.01	0.01	0.01	0.01	0.02	0.39	0.00	0.02
	UN_2	180	−19.10	0.02	0.00	0.00	0.00	0.00	0.00	0.07	0.09	0.79	0.00	0.01
		120	−17.16	0.01	0.02	0.12	0.03	0.02	0.02	0.02	0.05	0.68	0.00	0.01
HOMO-8	UO_2^{2+}	180	−40.48	0.00	0.00	0.00	0.03	0.00	0.00	0.04	0.06	0.85	0.00	0.01
		120	−41.10	0.01	0.11	0.45	0.00	0.01	0.01	0.00	0.02	0.37	0.02	0.01
	UN_2	180	−23.09	0.00	0.00	0.98	0.00	0.00	0.00	0.00	0.00	0.00	0.00	0.02
		120	−23.91	0.00	0.02	0.84	0.00	0.00	0.00	0.00	0.01	0.10	0.01	0.02

between HOMO−8 and HOMO−7, and the latter becomes more unstable at 120 degrees (Figure 8). Meanwhile, for UN_2, HOMO−8 and HOMO−7 are energetically farther, and the destabilization of HOMO−7 is weaker. We also observe that the sum of the populations of U's $6p_{3/2}$ and N's $2s_{1/2}$ in UN_2 shown in Figure 8 are less than that in ${UO_2}^{2+}$. From Table 3, this can be attributed to the larger contributions from $7s$ and $6d$, especially for the HOMO−7 of the linear UN_2. Although the splitting of the U's $6p_{3/2}$ peak caused by ligands has been experimentally observed,[76,77] the contribution of U's $6p_{3/2}$ to the molecular structure is reported for the first time.

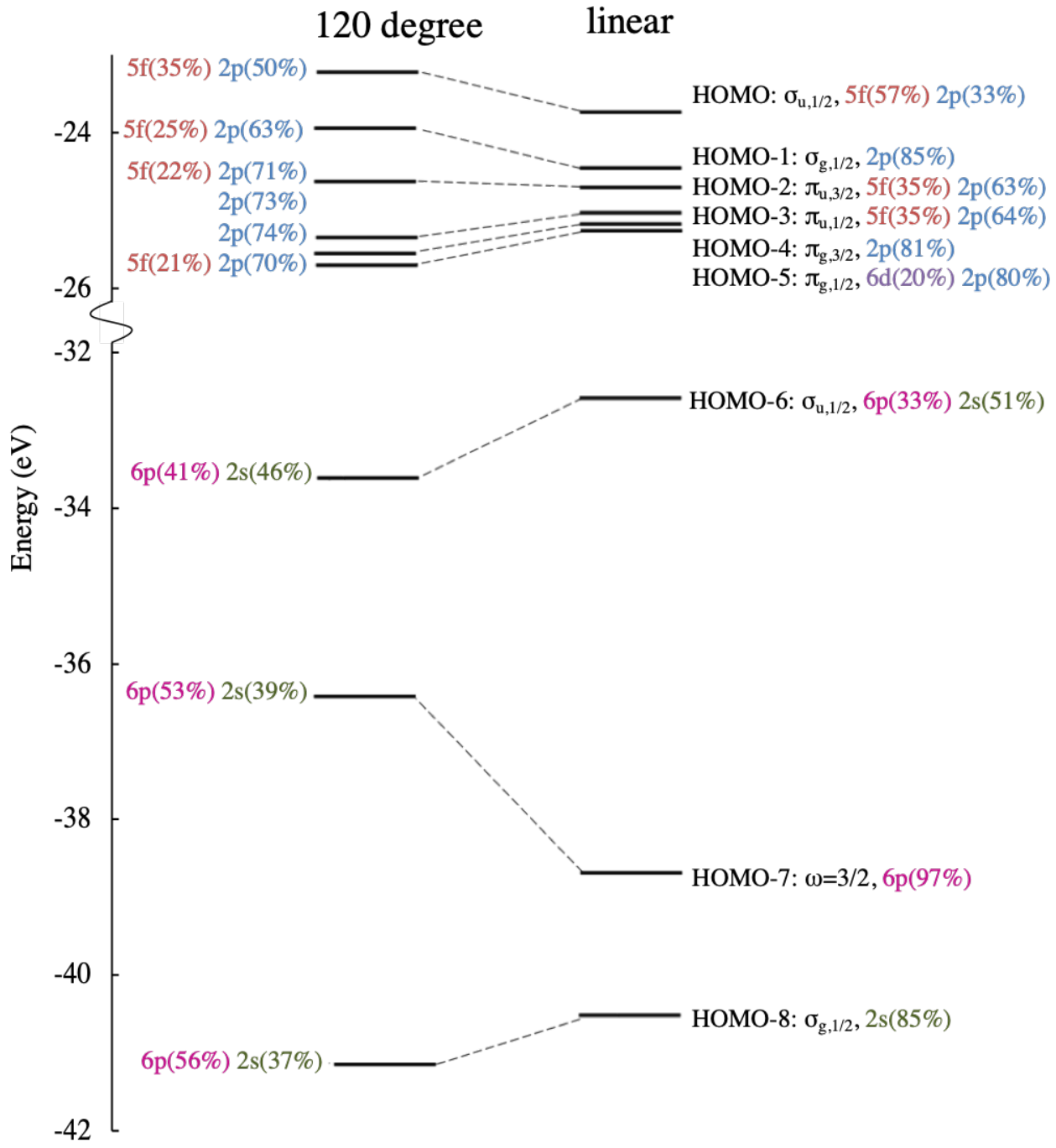

Figure 5: Walsh diagrams for UO_2^{2+} (R = 1.704 Å) for the nine highest occupied orbitals. The dominant contributions of the atomic orbitals provided in Table S1 are also shown.

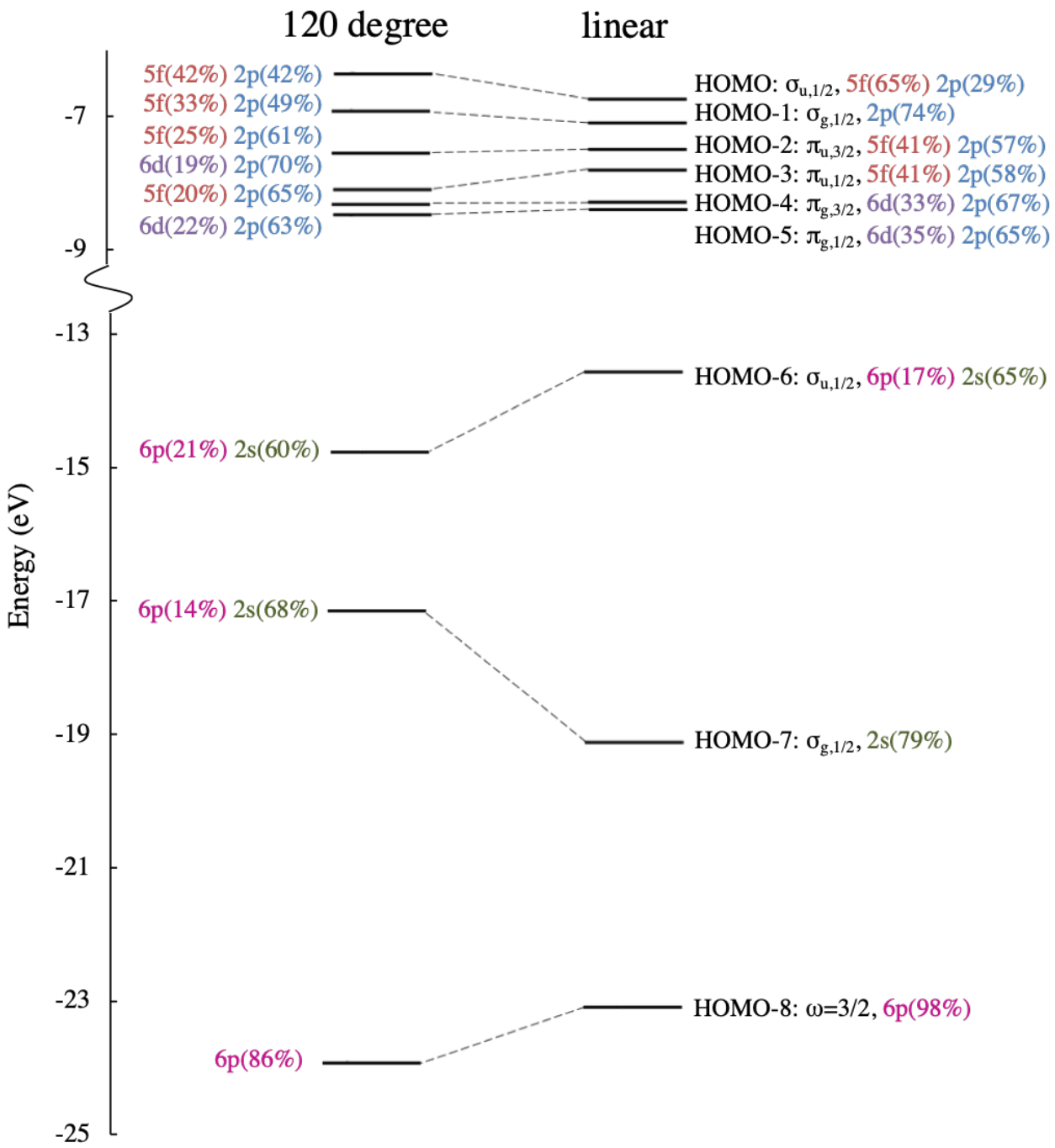

Figure 6: Walsh diagrams for UN_2 (R = 1.736 Å) for the nine highest occupied orbitals. The dominant contributions of the atomic orbitals provided in Table S2 are also shown.

Although estimating the accuracy of our analysis is not straightforward since the photospectroscopic on bare UO_2^{2+} and UN_2 do not exist, we can provide some remarks on

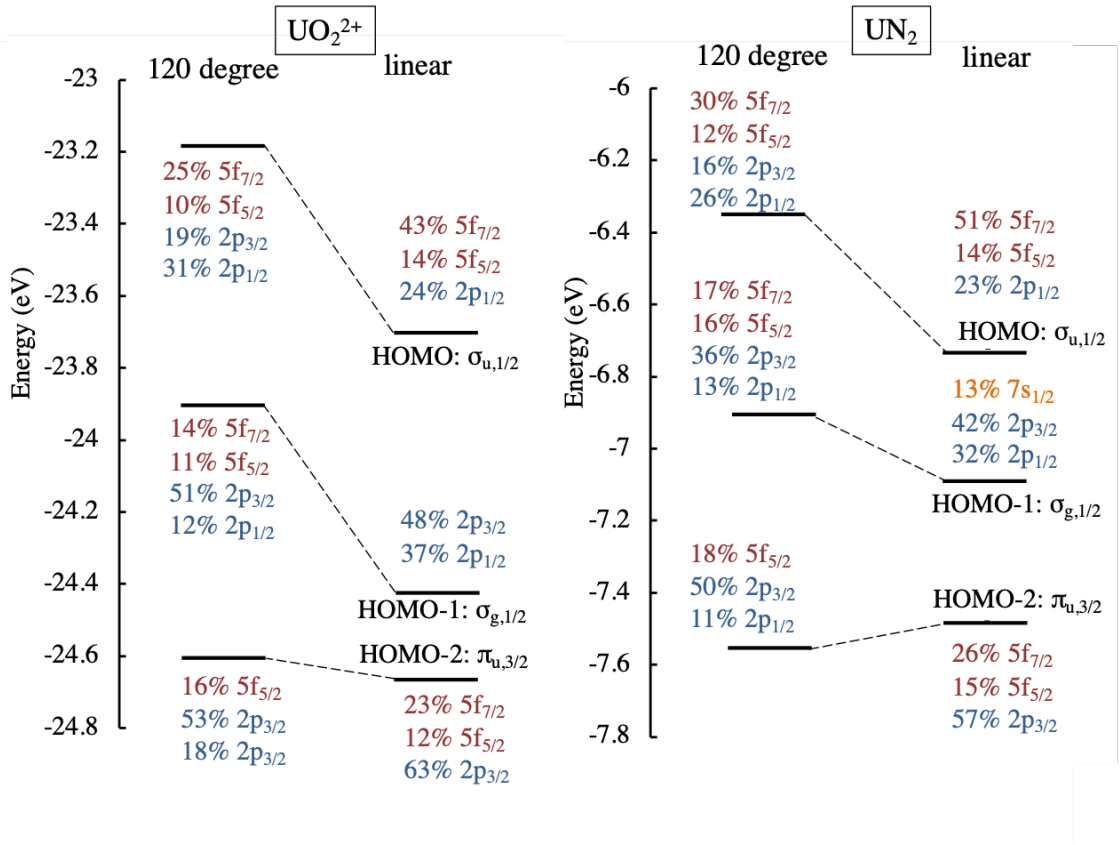

Figure 7: Walsh diagrams for UO_2^{2+} (R = 1.704 Å) and UN_2 (R = 1.736 Å) for the highest three occupied orbitals. The dominant contributions of atomic orbitals provided in Table 2 are also displayed. These are the highlights of Figures 5 and 6.

the accuracy. The order of the valence orbitals has not been clear for many years,[14,15] but that obtained by the ECP-DFT calculation[43] agrees with the photospectroscopic results of UO_2^{2+} in $Cs_2UO_2Cl_4$ crystals.[15] Our result in Figure 7, $\sigma_u >> \sigma_g > \pi_u$, agrees with these trends. The characteristic unstabilized HOMO has been explained using the pushing-from-below mechanism, which is a repulsive interaction between a filled-$6p_{3/2}$-main MO and a filled-HOMO.[14,26,43] However, reliable analyses by using a SO-included method and a basis set-independent population analysis have not been reported. Our population analysis shows that the contribution of $6p_{3/2}$ in HOMO is larger than those in the HOMO-1 and HOMO-2 for UO_2^{2+} (Table 2). For UN_2 the energy difference between HOMO and HOMO-1 is smaller than UO_2^{2+}, and the contribution of $6p_{3/2}$ is smaller than that in UO_2^{2+}. Our results are

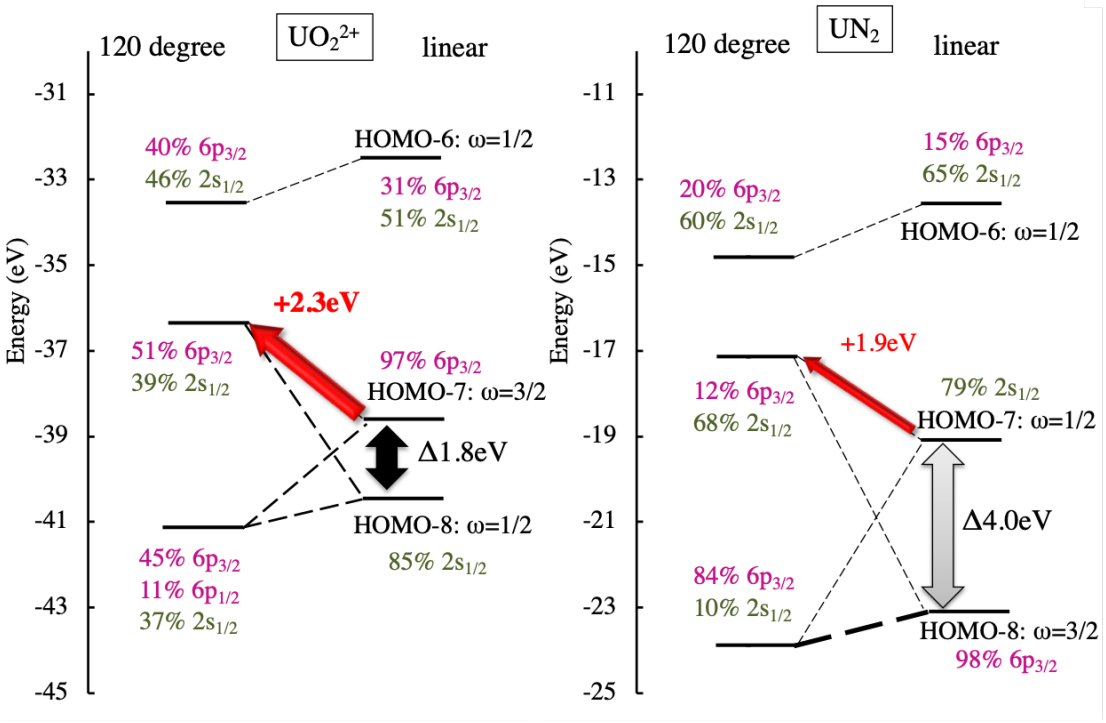

Figure 8: Walsh diagrams for UO_2^{2+} (R = 1.704 Å) and UN_2 (R = 1.736 Å) for no. 47-45 occupied orbitals. The dominant contributions of atomic orbitals provided in Table 3 are also displayed.

consistent with the prediction of the pushing-from-below mechanics.

Slightly bent structures

The slightly bent structures are also more stable than those expected at the HF level. The CCSD(T) results show that the destabilization energies at 170 degrees are 0.035 eV and 0.010 eV for UO_2^{2+} and UN_2, respectively, while the HF method overestimates the destabilization energies by 0.028 eV (Figure 9). The agreement between the results for the CCSD(T) and PBE0 levels implies that the PBE0 functional is suitable for accurately estimating UO_2^{2+} and UN_2 in slightly bent structures.

Like the destabilization energies, the U-X bond length does not vary with bending. Table 4 summarizes the optimized bond lengths at fixed bond angles and the destabilization energies obtained at these optimized bond lengths. The U-X (X = N, O) bond lengths increase

with the increase in the destabilization energy ΔE_{bent}, while the change in the U-O bond of UO_2^{2+} is only 0.003 Å for the 150-degree structure. From the above results, the model in our study, where the bond length is fixed and the angle is changed, would work well. The widely observed bent O-U-O angles in uranyl complexes, which are 160 degrees or larger,[54] are thermodynamically reasonable from the energetic order of magnitude shown in Table 4.

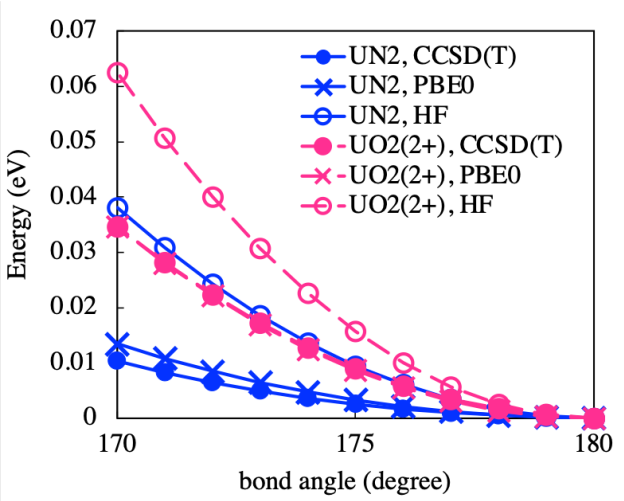

Figure 9: The destabilization of the total energies in the linear structure of UN_2 and UO_2^{2+} at the CCSD(T), PBE0, and HF levels as a function of angle (from 180 to 171 degrees). The U-X (X = N, O) bond lengths are fixed: 1.736 Å and 1.704 Å for UN_2 and UO_2^{2+}, respectively. This is the highlight of Figure 2.

Table 4: Optimized U-X (X = O, N) bond lengths at various angles and the destabilized energy (E_{bent}) from the linear structure at the optimized geometry. The PBE0 functional is employed.

	UO_2^{2+}		UN_2	
Angle (degree)	r_e(Å)	ΔE_{bent} (eV)	r_e(Å)	ΔE_{bent}(eV)
150	1.687	0.323	1.717	0.149
155	1.685	0.225	1.716	0.098
160	1.684	0.144	1.716	0.059
165	1.684	0.081	1.716	0.032
170	1.683	0.036	1.716	0.014
175	1.683	0.009	1.716	0.003
180	1.683	0.000	1.716	0.000

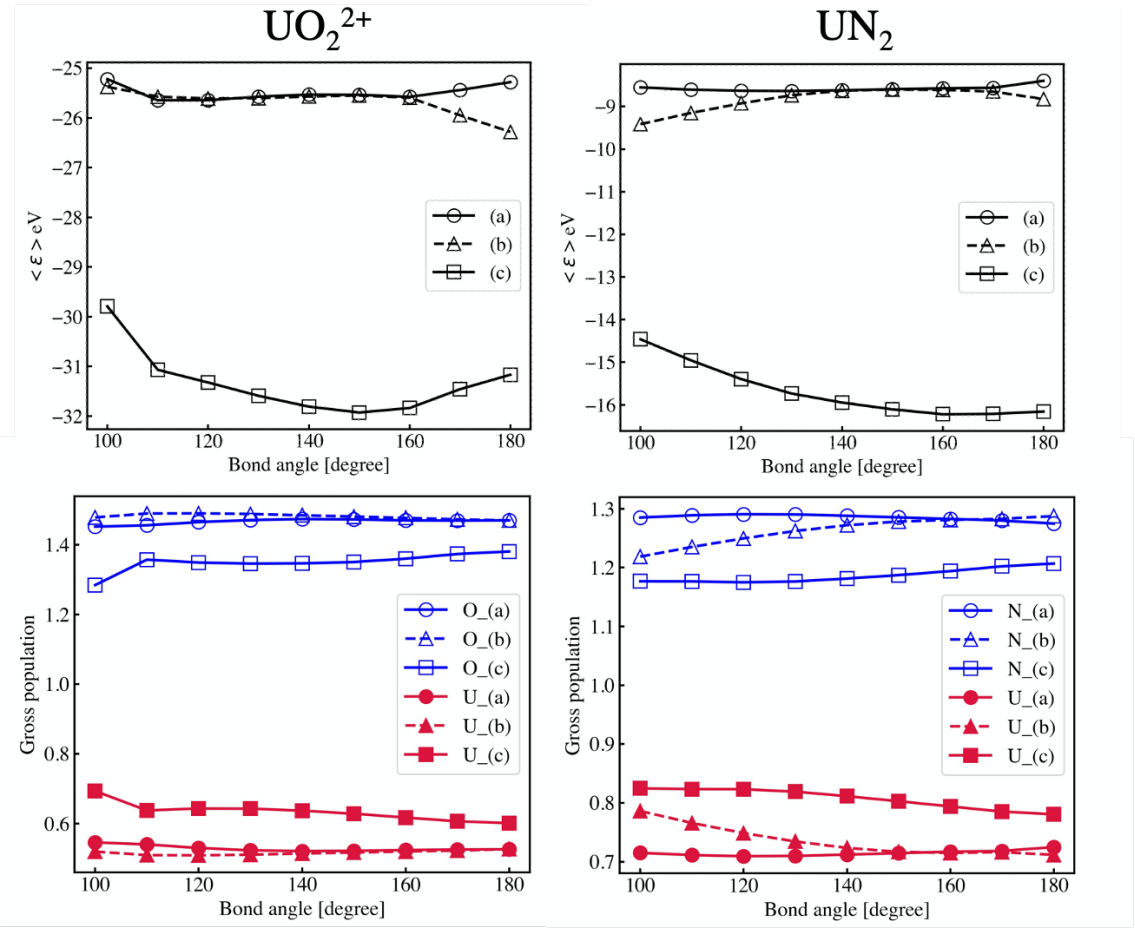

Figure 10: Expectation values of the Fock matrix $< \varepsilon >$ (the upper figures) and the projection analysis of the localized bonding orbitals (the lower figures) as a function of angle (from 180 to 100 degrees) at the PBE0 level. (a), (b), and (c) are the labels of the localized bonding orbitals.

Chemical bonds

The above rigid U-X (X = N, O) bond length with respect to the change in the angle can be attributed to the conservation of the chemical bonds. The triple bond in U-X, which consists of two pseudo-degenerate bonds and an energetically stable bond, remains unbroken even at 100 degrees (Figure 10). The composition of each atom does not significantly change as the angle decreases. The features of UO_2^{2+} and UN_2 are almost identical, whereas the chemical bonds in UO_2^{2+} are more ionic than those in UN_2.

The compositions of the LMOs remain fairly unchanged with change in angle, as the

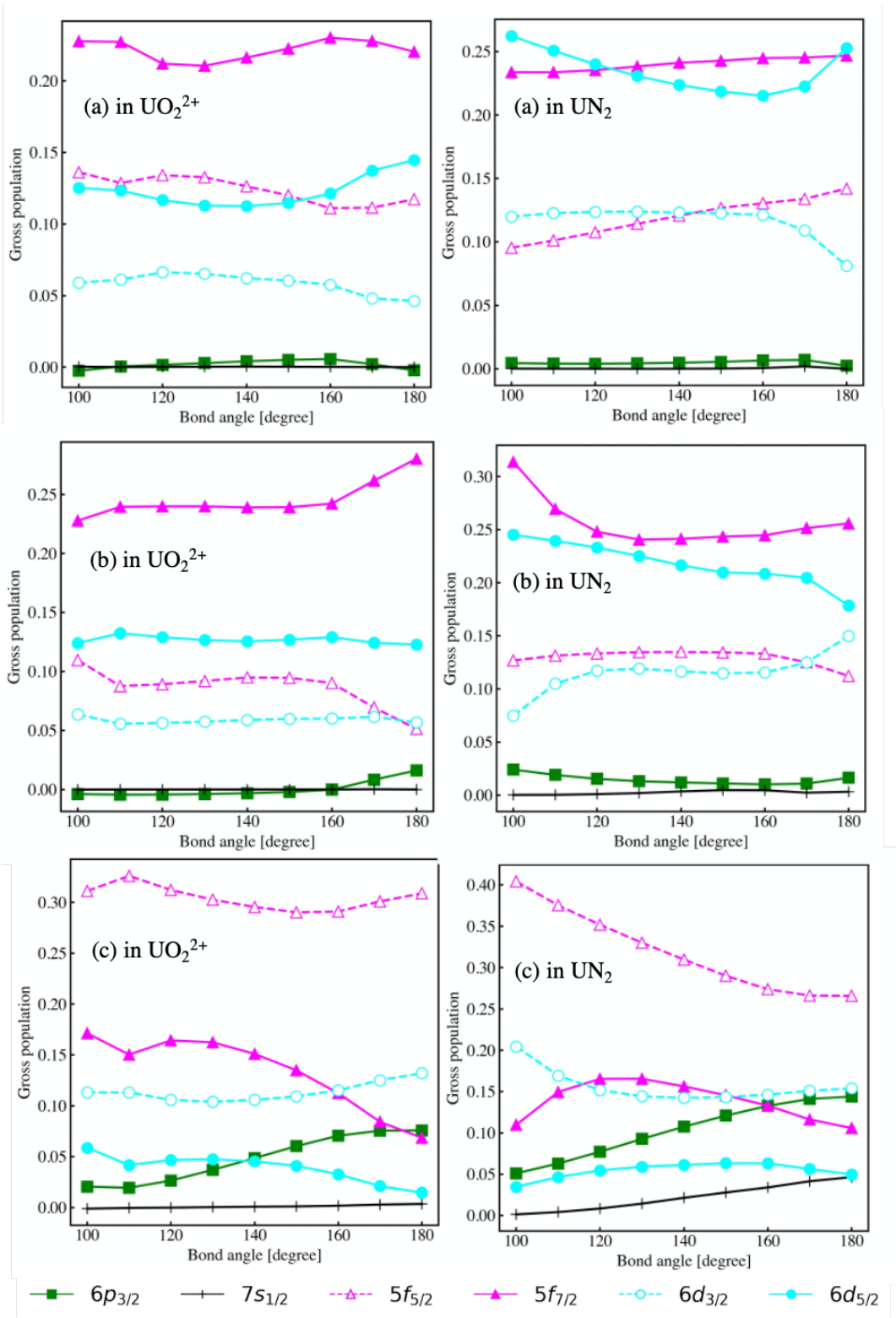

Figure 11: Contributions of each atomic orbital obtained with projection analysis of the localized bonding orbitals as a function of angle (from 180 to 100 degrees) at the PBE0 level. The occupation number two is multiplied. The expectation value of the Fock matrix $< \varepsilon >$ for orbitals (a), (b), and (c) are given in Figure 10.

maximum change in the population does not exceed 0.15 (Figure 11). However, we can provide some remarks: i) For both UO_2^{2+} and UN_2, the $5f_{7/2}$ and $6d_{5/2}$ orbitals contribute more than $5f_{5/2}$ and $6d_{3/2}$ orbitals in LMOs (a) and (b). Meanwhile, the contributions of $5f_{5/2}$ and $6d_{3/2}$ orbitals are prominent in the LMO (c). This distinct difference is not found in ref.,[46] where the calculations of the linear UO_2^{2+}, UNO^+, and UN_2 were performed at the DCG-HF level. ii) The contributions of d orbitals in UN_2 are larger than those in UO_2^{2+}. This is because the promotion from $5f$ to $7s$ in *cationic* UO_2^{2+} takes more energy than that in the UN_2. iii) In the LMO (c), the contributions of $6p_{3/2}$ are relatively large for both linear UO_2^{2+} and UN_2, but it decreases as the angle becomes smaller. On the contrary, the contributions from $5f_{7/2}$ increases in UO_2^{2+}, whereas $5f_{5/2}$ becomes more dominant in UN_2.

Comparison with linear UE_2^{2+} (E = S, Se, Te)

Referring to the above discussion on UO_2^{2+} and UN_2, we analyze more costly systems, UE_2^{2+} (E = S, Se, Te). From theoretical studies, triangle-type $U\cdots S_2$ isomer is more stable than its linear structure.[78,79] Note that the structure of the triangle-type US_2^{+2} with S-S and U-S bonds is different from the bent structure, wherein the U-S bond is generated, but the S-S bond is not. However, our purpose is the comparison between UE_2^{2+} and UO_2^{2+} whose electronic ground state is the linear structure. The analysis of the linear-type UE_2^{2+} can give another insight of UO_2^{2+} molecule. The linear structure of UE_2^{2+} is analyzed in ref.,[80] but only their valence orbitals are analyzed and the spin-orbit coupling is not taken into account here. Although OUS^+ cation[81] and complexes that consist of the linear OUE^{2+}[82] have been also synthesized, we focus on only triatomic systems with D_∞ symmetry in this study.

Although both the models based on the valence and core-valence orbitals work well for UO_2^{2+} and UN_2, the latter works much better for UE_2^{2+}. The correct set of the MOs that captures the dominant effect is "HOMO−7 - HOMO−8", although for UTe_2^{2+} the agreement

is slightly bad (Table 5). The orbital energies and the charge population of the target MOs are summarized in Figures 12-14 and Tables S3-S5. For US_2^{2+} and USe_2^{2+}, the destabilization of the ns-main MO (n is the principal quantum number of the valence shell of the chalcogen) at 120 degrees mainly stabilizes the linear structure. For UTe_2^{2+}, the stabilization of $6p_{3/2}$ at 120 degrees stabilizes the bent structure. The population of HOMO$-$7 and HOMO$-$8 for the linear and bent structures are similar since these MO are energetically separated and the MOs are not mixed so much. The similarity between UO_2^{2+} and UE_2^{2+} is that $6p_{3/2}$ and ns dominate MO contributions to the the molecular structures. The difference between the order of $6p_{3/2}$ and ns dominant MOs in UO_2^{2+} and UE_2^{2+} can be explained by the much lower AO energy of O $2s$: the ns AO energies for O, S, Se, and Te are, -27.1 eV, -19.4 eV, -19.2 eV, and -16.8 eV, respectively, at the DCG-PBE0 level.

Table 5: Destabilized energy (eV) at 120 degrees compared to that at 180 degrees for UE_2^{2+} (E = S, Se, Te) at the PBE0 level. "n - m" refers to the sum of the orbital energies from n^{th} to m^{th} KS orbitals at the PBE0 level. The negative value means the 120-degree structure is more stable. The correspondence to Table 1 is given in the caption.

	US_2^{2+}	USe_2^{2+}	UTe_2^{2+}
total energy	0.590	0.378	-0.729
HOMO - HOMO$-$7	-0.156	-0.273	0.349
HOMO - HOMO$-$2	0.234	-0.089	-0.203
HOMO$-$6 - HOMO$-$7	0.057	-0.057	0.408
HOMO$-$7 - HOMO$-$8	0.394	0.337	-0.227

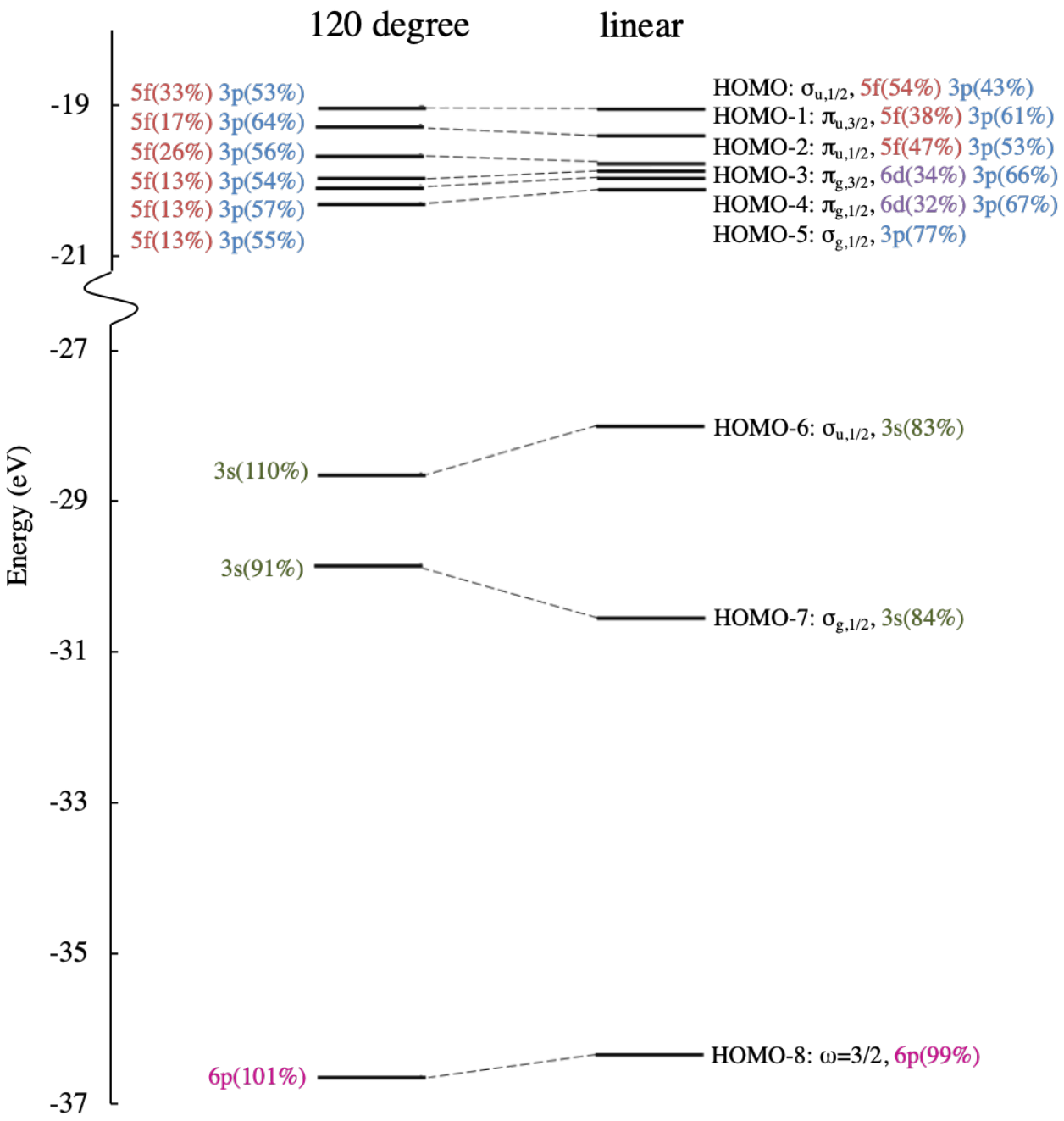

Figure 12: Walsh diagrams for US_2^{2+} (R = 2.190 Å) for the nine highest occupied orbitals. The dominant contributions of the atomic orbitals provided in Table S3 are also shown.

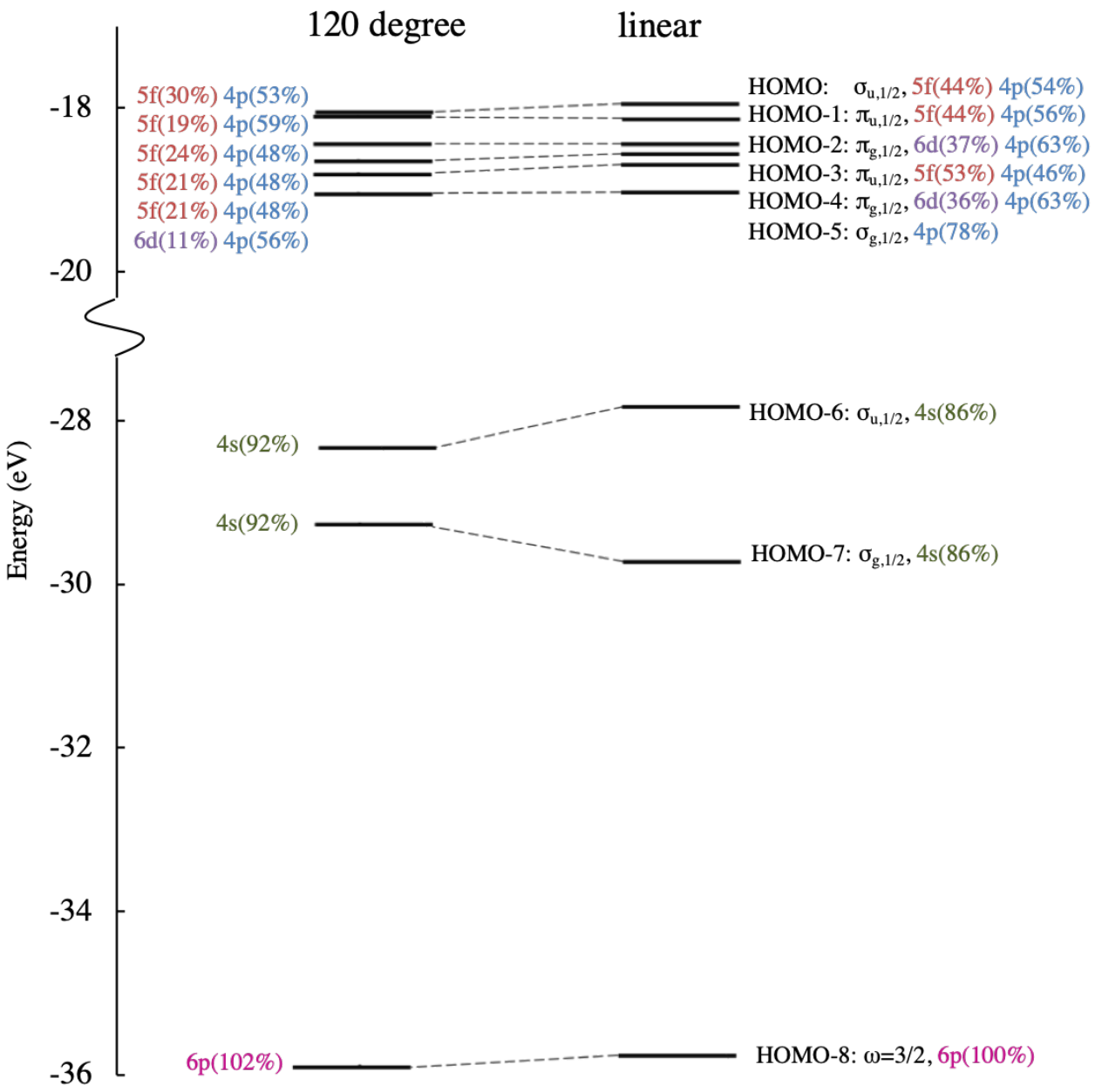

Figure 13: Walsh diagrams for USe_2^{2+} ($R = 2.358$ Å) for the nine highest occupied orbitals. The dominant contributions of the atomic orbitals provided in Table S4 are also shown.

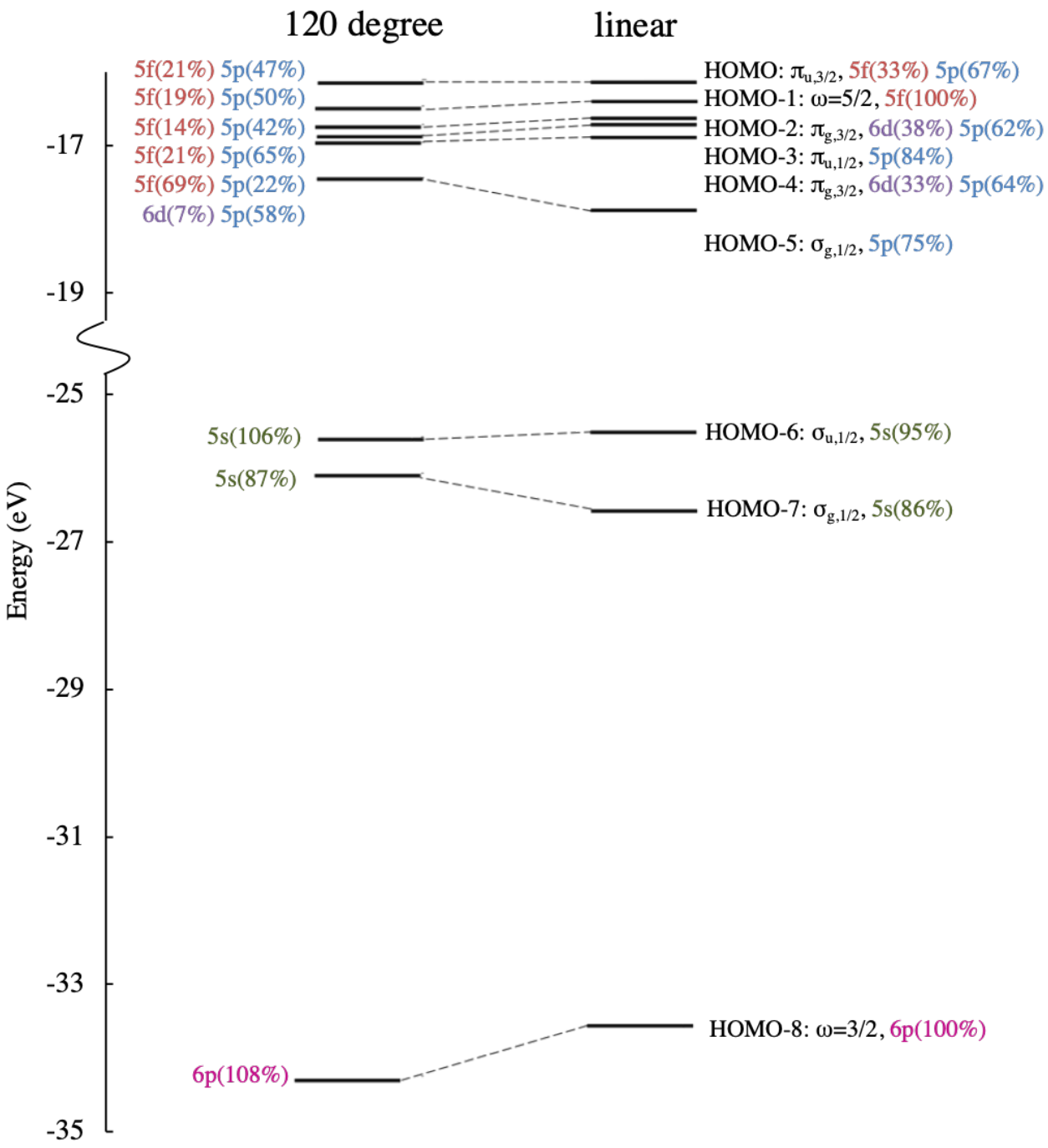

Figure 14: Walsh diagrams for UTe_2^{2+} ($R = 2.680$ Å) for the nine highest occupied orbitals. The dominant contributions of the atomic orbitals provided in Table S5 are also shown.

When comparing the charge population of UO_2^{2+} and UE_2^{2+}, some trends that cannot be simply explained by electronegativity are observed. From Table 6 the values of $<\varepsilon>$ increases

as with heavier chalcogens, indicating that the triple bonds in UE_2^{2+} are unstable. The trends of the population of US_2^{2+} and USe_2^{2+} are similar to that of UO_2^{2+}, but the population transfer from $5f_{5/2}$ to $5f_{7/2}$ increases with heavier chalcogens (Table 7). Finally, for UTe_2^{2+}, the lowest energy bonding-type LMO is split to two LMOs, a $5f_{5/2}$-dominant lone-pair-type LMO, and the bond distributed to the two Te atoms: i.e., two Te atoms contribute to the one LMO (Table 6). As expected from the electronegativity of the chalcogen, the charge of U decreases with heavier chalcogens, and only in UO_2^{2+} the charge of U increase beyond the system's charge (+2, Table 7). From the comparison between UO_2^{2+} and UE_2^{2+}, the $6p$ hole[83] becomes significant only in UO_2^{2+}.

Table 6: Projection analysis of the localized bonding-type and lone-pair-type KS orbitals of US_2^{2+} (R = 2.190 Å), USe_2^{2+} (R = 2.358 Å) and UTe_2^{2+} (R = 2.680 Å). $<\varepsilon>$ is the expectation value of the Fock operator. E refers to O, S, Se or Te atoms. For UTe_2^{2+}, two Te atoms equally contributes to the lowest energy LMO, and the highest energy LMO is the lone-pair type orbital. The other LMOs are doubly degenerated.

mol.	$<\varepsilon>$ eV	ω	U6s$_{1/2}$	U6p$_{1/2}$	U6p$_{3/2}$	U5f$_{5/2}$	U5f$_{7/2}$	U6d$_{3/2}$	U6d$_{5/2}$	U7s$_{1/2}$	Ens$_{1/2}$	Enp$_{1/2}$	Enp$_{3/2}$
UO_2^{2+}	-31.17	1/2	-0.01	0.01	0.04	0.15	0.03	0.07	0.01	0.00	0.00	0.03	0.66
	-26.28	1/2	0.00	0.00	0.01	0.03	0.14	0.03	0.06	0.00	0.00	0.70	0.04
	-25.28	3/2	0.00	0.00	0.00	0.06	0.11	0.02	0.07	0.00	0.00	0.00	0.74
US_2^{2+}	-24.53	1/2	-0.01	0.01	0.03	0.20	0.07	0.10	0.03	0.01	0.00	0.07	0.48
	-20.25	1/2	0.00	0.00	0.00	0.04	0.14	0.07	0.10	0.00	0.00	0.58	0.08
	-19.87	3/2	0.00	0.00	0.00	0.09	0.10	0.04	0.13	0.00	0.00	0.00	0.64
USe_2^{2+}	-21.96	1/2	0.00	0.01	0.02	0.26	0.03	0.14	0.01	0.01	0.00	0.01	0.51
	-19.69	1/2	0.00	0.00	0.00	0.01	0.15	0.03	0.12	0.00	0.00	0.67	0.02
	-18.54	3/2	0.00	0.00	0.00	0.12	0.09	0.05	0.14	0.00	0.00	0.00	0.60
UTe_2^{2+}	-21.75	1/2	-0.01	0.00	0.00	0.00	0.00	0.25	0.06	0.09	0.00	0.03,0.03	0.27,0.27
	-17.96	1/2	0.00	0.00	0.00	0.03	0.05	0.05	0.09	0.00	0.01	0.68	0.07
	-16.64	3/2	0.00	0.00	0.00	0.08	0.08	0.05	0.14	0.00	0.00	0.00	0.65
	-16.36	5/2	0.00	0.00	0.00	0.95	0.05	0.00	0.00	0.00	0.00	0.00	0.00

Table 7: Charge of U atom (Q) and atomic configuration in the title compounds at the linear structure obtained via projection analysis.

	Q	U	chalcogen
UO_2^{2+}	2.52	$6p_{1/2}^{1.95}6p_{3/2}^{3.76}$ $5f_{5/2}^{1.19}5f_{7/2}^{1.48}$ $7s_{1/2}^{0.04}$ $6d_{3/2}^{0.49}6d_{5/2}^{0.59}$	$2s_{1/2}^{1.90}$ $2p_{1/2}^{1.47}2p_{3/2}^{2.88}$
US_2^{2+}	1.38	$6p_{1/2}^{1.98}6p_{3/2}^{3.90}$ $5f_{5/2}^{1.45}5f_{7/2}^{1.41}$ $7s_{1/2}^{0.05}$ $6d_{3/2}^{0.83}6d_{5/2}^{1.02}$	$3s_{1/2}^{1.91}$ $3p_{1/2}^{1.32}3p_{3/2}^{2.46}$
USe_2^{2+}	1.21	$6p_{1/2}^{1.98}6p_{3/2}^{3.93}$ $5f_{5/2}^{1.70}5f_{7/2}^{1.17}$ $7s_{1/2}^{0.08}$ $6d_{3/2}^{0.88}$ $6d_{5/2}^{1.05}$	$4s_{1/2}^{1.93}$ $4p_{1/2}^{1.38}4p_{3/2}^{2.29}$
UTe_2^{2+}	0.98	$6p_{1/2}^{1.99}6p_{3/2}^{3.96}$ $5f_{5/2}^{2.34}5f_{7/2}^{0.65}$ $7s_{1/2}^{0.17}$ $6d_{3/2}^{0.88}6d_{5/2}^{1.02}$	$5s_{1/2}^{1.94}$ $5p_{1/2}^{1.50}5p_{3/2}^{2.05}$

CONCLUSIONS

Herein, the structures and chemical bonds of UO_2^{2+} and those of UN_2 and UE_2^{2+} (E = S, Se, Te) were compared based on relativistic calculations. In previous studies, the valence molecular orbitals were employed to analyze their linear structures, whereas we formulated another mechanism based on the core-valence orbitals herein. Destabilization of U $6p_{3/2}$ orbitals in the bent structure prevents the bending of UO_2^{2+} to a larger extent than for UN_2. For UE_2^{2+}, core-valence orbitals (i.e., U's $6p_{3/2}$ and ns main MOs) contribute to the molecular structure. Meanwhile, the charge population of the U $6p_{3/2}$-dominant MOs were largely unchanged even in the 120 degrees structure, and the $6p$ hole was very small for UE_2^{2+}. The bond lengths of UO_2^{2+} and UN_2 remain rigid as the structure bends, which can be attributed to the approximately constant triple bonds between U and X in the bent structure. Meanwhile, the triple bond weakened with heavier chalcogens. In the extreme case, UTe_2^{2+}, one of the bonding-type LMO is broken and $5f_{5/2}$-dominant lone-pair-type LMO appears. From the above comparison, two unique features of UO_2^{2+} in the uranium chalcogen systems arose: i) the contribution of $6p_{3/2}$ to the orbital interaction along with a decreased occupation number of $6p_{3/2}$ and ii) rigid triple bonds even in the bent structures.

In this study, we analyzed "bare" molecules that directly correspond to the experiments in gas phase.[84–86] This analysis would be applicable even for complexes in which the ligand field is very weak. When the electronic structure of UO_2^{2+} in a complex resembles that of the bare one and steric repulsion is dominant, our analysis reveals that UO_2^{2+} can bend more easily compared to the conventional prediction based on the HF method. Further research is required for systems with strong ligand fields. Our analysis of the U's $6p_{3/2}$ orbital encourages us to re-investigate the structure of uranium complexes.

Acknowledgement

A.S. thank financial support received from the Japan Society for the Promotion of Science (JSPS) KAKENHI (Grant No. 20K22553 and 21K14643). We are also thankful for use of the supercomputers of ACCMS (Kyoto University) and Research Institute for Information Technology, Kyushu University (General Projects). We thank Editage (www.editage.com) for English language editing.

Supporting Information Available

The supporting information contains the summary of the projection analysis for the nine highest canonical occupied orbitals of the studied molecules in this work.

References

(1) Gagliardi, L.; Roos, B. O. Uranium triatomic compounds XUY (X,Y=C,N,O): a combined multiconfigurational second-order perturbation and density functional study. *Chem. Phys. Lett.* **2000**, *331*, 229–234.

(2) Wang, X.; Andrews, L.; Vlaisavljevich, B.; Gagliardi, L. Combined triple and double bonds to uranium: the N≡U=N-H uranimine nitride molecule prepared in solid argon. *Inorg. Chem.* **2011**, *50*, 3826–3831.

(3) Hu, H. S.; Qiu, Y. H.; Xiong, X. G.; Schwarz, W. H. E.; Li, J. On the maximum bond multiplicity of carbon: Unusual C≡U quadruple bonding in molecular CUO. *Chem. Sci.* **2012**, *3*, 2786–2796.

(4) Hayton, T. W. Recent developments in actinide-ligand multiple bonding. *Chem. Commun.* **2013**, *49*, 2956–2973.

(5) Hu, H.-S.; Wei, F.; Wang, X.; Andrews, L.; Li, J. Actinide-silicon multiradical bonding: infrared spectra and electronic structures of the Si(μ-X)AnF$_3$ (An = Th, U; X = H, F) molecules. *J. Am. Chem. Soc.* **2014**, *136*, 1427–1437.

(6) Ruipérez, F.; Merino, G.; Ugalde, J. M.; Infante, I. Molecules with high bond orders and ultrashort bond lengths: CrU, MoU, and WU. *Inorg. Chem.* **2013**, *52*, 2838–2843.

(7) Hlina, J. A.; Pankhurst, J. R.; Kaltsoyannis, N.; Arnold, P. L. Metal-Metal Bonding in Uranium-Group 10 Complexes. *J. Am. Chem. Soc.* **2016**, *138*, 3333–3345.

(8) Chi, C.; Wang, J.-Q.; Qu, H.; Li, W.-L.; Meng, L.; Luo, M.; Li, J.; Zhou, M. Preparation and Characterization of Uranium-Iron Triple-Bonded UFe(CO)$_3$- and OUFe(CO)$_3$-Complexes. *Angew. Chem. Int. Ed Engl.* **2017**, *56*, 6932–6936.

(9) Lu, E.; Wooles, A. J.; Gregson, M.; Cobb, P. J.; Liddle, S. T. A very short uranium(IV)–rhodium(I) bond with net double-dative bonding character. *Angew. Chem. Weinheim Bergstr. Ger.* **2018**, *130*, 6697–6701.

(10) Roos, B. O.; Malmqvist, P.-Å.; Gagliardi, L. Exploring the Actinide–Actinide Bond: Theoretical Studies of the Chemical Bond in Ac_2 , Th_2 , Pa_2 , and U_2. *J. Am. Chem. Soc.* **2006**, *128*, 17000–17006.

(11) Ciborowski, S. M.; Mitra, A.; Harris, R. M.; Liu, G.; Sharma, P.; Khetrapal, N.; Blankenhorn, M.; Gagliardi, L.; Bowen, K. H. Metal-Metal Bonding in Actinide Dimers: U_2 and U_2. *J. Am. Chem. Soc.* **2021**, *143*, 17023–17028.

(12) Gagliardi, L.; Roos, B. O. Quantum chemical calculations show that the uranium molecule U2has a quintuple bond. *Nature* **2005**, *433*, 848–851.

(13) Knecht, S.; Jensen, H. J. A.; Saue, T. Relativistic quantum chemical calculations show that the uranium molecule U_2 has a quadruple bond. *Nat. Chem.* **2019**, *11*, 40–44.

(14) Pepper, M.; Bursten, B. E. The electronic structure of actinide-containing molecules: a challenge to applied quantum chemistry. *Chem. Rev.* **1991**, *91*, 719–741.

(15) Denning, R. G. *Complexes, Clusters and Crystal Chemistry*; Springer Berlin Heidelberg: Berlin, Heidelberg, 1992; pp 215–276.

(16) Denning, R. G. Electronic structure and bonding in actinyl ions and their analogs. *J. Phys. Chem. A* **2007**, *111*, 4125–4143.

(17) Fortier, S.; Hayton, T. W. Oxo ligand functionalization in the uranyl ion (UO_2^{2+}). *Coord. Chem. Rev.* **2010**, *254*, 197–214.

(18) Jong, W. F. D. Over De Kristalstructuur Van Natrium-Uranylacetaat. *Physica* **1930**, *10*, 101–108.

(19) Fankuchen, I. Crystal Structure of Sodium Uranyl Acetate. *Z. Kristallogr. Cryst. Mater.* **1935**, *91*, 473–479.

(20) Glueckauf, E.; McKAY, H. A. C. Possible F-Shell Covalency in the Actinide Elements. *Nature* **1950**, *165*, 594–595.

(21) Katzin, L. I. Possible f-Shell Covalency in the Actinide Elements. *Nature* **1950**, *166*, 605–605.

(22) Glueckauf, E.; McKAY, H. A. C. Possible f-Shell Covalency in the Actinide Elements. *Nature* **1950**, *166*, 605–606.

(23) Eisenstein, J. C.; Pryce, M. H. L. The electronic structure and magnetic properties of uranyl-like ions I. Uranyl and neptunyl. *Proc. R. Soc. Lond. A Math. Phys. Sci.* **1955**, *229*, 20–38.

(24) Walch, P. F.; Ellis, D. E. Effects of secondary ligands on the electronic structure of uranyls. *J. Chem. Phys.* **1976**, *65*, 2387–2392.

(25) Yang, C. Y.; Johnson, K. H.; Horsley, J. A. Relativistic Xα–scattered-wave calculations for the uranyl ion. *J. Chem. Phys.* **1978**, *68*, 1001–1005.

(26) Tatsumi, K.; Hoffmann, R. Bent Cis d^0 MoO_2^{2+} vs. Linear Trans d^0f^0 UO_2^{2+}: A Significant Role for Nonvalence 6p Orbitals in Uranyl. *Inorg. Chem.* **1980**, *19*, 2656–2658.

(27) Wood, J. H.; Boring, M.; Woodruff, S. B. Relativistic electronic structure of UO_2^{++}, UO_2^+, and UO_2. *J. Chem. Phys.* **1981**, *74*, 5225–5233.

(28) Pyykkö, P.; Lohr, L. L. Relativistically Parameterized Extended Hückel Calculations. 3. Structure and Bonding for Some Compounds of Uranium and Other Heavy Elements. *Inorg. Chem.* **1981**, *20*, 1950–1959.

(29) Boring, M.; Wood, J. H. A note on SCF calculations of valence levels in heavy molecules. *J. Chem. Phys.* **1979**, *71*, 392–399.

(30) Wadt, W. R. Why uranyl ion(2+) is linear and isoelectronic thorium dioxide is bent. *J. Am. Chem. Soc.* **1981**, *103*, 6053–6057.

(31) de Jong, W. A.; Visscher, L.; Nieuwpoort, W. C. On the bonding and the electric field gradient of the uranyl ion1. *J. Mol. Struct.* **1999**, *458*, 41–52.

(32) Pierloot, K.; van Besien, E. Electronic structure and spectrum of UO_2^{2+} and $UO_2Cl_4^{2-}$. *J. Chem. Phys.* **2005**, *123*, 204309.

(33) Real, F.; Gomes, A. S. P.; Visscher, L.; Vallete, V.; Eliav, E. Benchmarking electronic structure calculations on the bare UO_2^{2+} ion: How different are single and multireference electron correlation methods? *J. Phys. Chem. A* **2009**, *113*, 12504–12511.

(34) Tecmer, P.; Gomes, A. S. P.; Ekström, U.; Visscher, L. Electronic spectroscopy of UO_2^{2+}, NUO^+ and NUN: An evaluation of time-dependent density functional theory for actinides. *Phys. Chem. Chem. Phys.* **2011**, *13*, 6249–6259.

(35) Tecmer, P.; Severo Pereira Gomes, A.; Knecht, S.; Visscher, L. Communication: Relativistic Fock-space coupled cluster study of small building blocks of larger uranium complexes. *J. Chem. Phys.* **2014**, *141*, 041107.

(36) McGlynn, S. P.; Smith, J. K.; Neely, W. C. Electronic Structure, Spectra, and Magnetic Properties of Oxycations. III. Ligation Effects on the Infrared Spectrum of the Uranyl Ion. *J. Chem. Phys.* **1961**, *35*, 105–116.

(37) Bist, H. D. The far infrared spectra of uranyl salts. *J. Mol. Spectrosc.* **1968**, *27*, 542–544.

(38) Bullock, J. I.; Parrett, F. W. The low frequency infrared and Raman spectroscopic studies of some uranyl complexes: the deformation frequency of the uranyl ion. *Can. J. Chem.* **1970**, *48*, 3095–3097.

(39) Cattalini, L.; Croatto, U.; Degetto, S.; Tondello, E. Uranyl chelate complexes. *Inorganica Chim. Acta* **1971**, *5*, 19–43.

(40) Pyykko, P.; Laaksonen, L. Relativistically parameterized extended Hueckel calculations. 8. Double-.zeta. parameters for the actinoids thorium, protactinium, uranium, neptunium, plutonium, and americium and an application on uranyl. *J. Phys. Chem.* **1984**, *88*, 4892–4895.

(41) Dyall, K. G. Bonding and bending in the actinyls. *Mol. Phys.* **1999**, *96*, 511–518.

(42) Vasiliu, M.; Jian, T.; Gibson, J. K.; Peterson, K. A.; Dixon, D. A. A Computational Assessment of Actinide Dioxide Cations AnO_2^{2+} for An = U to Lr: The Limited Stability Range of the Hexavalent Actinyl Moiety, $[O{=}An{=}O]^{2+}$. *Inorg. Chem.* **2020**, *59*, 4554–4566.

(43) Kaltsoyannis, N. Computational study of analogues of the uranyl ion containing the -N=U=N- unit: density functional theory calculations on UO_2^{2+}, UON^+, UN_2,

$UO(NPH_3)^{3+}$, $U(NPH3)_2^{4+}$, $[UCl_4[NPR_3]_2]$ (R = H, Me), and $[UOCl_4[NP(C_6H_5)_3]]$. *Inorg. Chem.* **2000**, *39*, 6009–6017.

(44) Han, Y.-K.; Hirao, K. Density functional studies of UO22+ and AnF6 (An=U, Np, and Pu) using scalar-relativistic effective core potentials. *J. Chem. Phys.* **2000**, *113*, 7345–7350.

(45) Kovács, A.; Konings, R. J. M. Computed vibrational frequencies of actinide oxides AnO(0/+/2+) and AnO_2(0/+/2+) (An = Th, Pa, U, Np, Pu, Am, Cm). *J. Phys. Chem. A* **2011**, *115*, 6646–6656.

(46) South, C.; Shee, A.; Mukherjee, D.; Wilson, A. K.; Saue, T. 4-Component relativistic calculations of L3 ionization and excitations for the i species UO_2^{2+}, OUN^+ and UN_2. *Phys. Chem. Chem. Phys.* **2016**, *18*, 21010–21023.

(47) Clavaguéra-Sarrio, C.; Ismail, N.; Marsden, C. J.; Bégué, D.; Pouchan, C. Calculation of harmonic and anharmonic vibrational wavenumbers for triatomic uranium compounds XUY. *Chem. Phys.* **2004**, *302*, 1–11.

(48) de Jong, W. A.; Harrison, R. J.; Nichols, J. A.; Dixon, D. A. Fully relativistic correlated benchmark results for uranyl and a critical look at relativistic effective core potentials for uranium. *Theor. Chem. Acc.* **2001**, *107*, 22–26.

(49) Jackson, V. E.; Craciun, R.; Dixon, D. A.; Peterson, K. A.; de Jong, W. A. Prediction of vibrational frequencies of UO_2^{2+} at the CCSD(T) level. *J. Phys. Chem. A* **2008**, *112*, 4095–4099.

(50) Vaughn, A. E.; Barnes, C. L.; Duval, P. B. Acis-Dioxido Uranyl: Fluxional Carboxylate Activation from a Reversible Coordination Polymer. *Angew. Chem. Int. Ed Engl.* **2007**, *119*, 6742–6745.

(51) Guan, Q. L.; Bai, F. Y.; Xing, Y. H.; Liu, J.; Zhang, H. Z. Unexpected cis-dioxido uranyl carboxylate compound: Synthesis, characterization and photocatalytic activity of uranyl-succinate complexes. *Inorg. Chem. Commun.* **2015**, *59*, 36–40.

(52) Villiers, C.; Thuéry, P.; Ephritikhine, M. The First cis -Dioxido Uranyl Compound under Scrutiny. *Angew. Chem. Int. Ed Engl.* **2008**, *120*, 5976–5977.

(53) Langer, E. M.; Kegler, P.; Kowalski, P. M.; Wang, S.; Alekseev, E. V. Achieving and Stabilizing Uranyl Bending via Physical Pressure. *Inorg. Chem.* **2021**, *60*, 8419–8422.

(54) Hayton, T. W. Understanding the origins of Oyl-U-Oyl bending in the uranyl (UO_2^{2+}) ion. *Dalton Trans.* **2018**, *47*, 1003–1009.

(55) Schöne, S.; Radoske, T.; März, J.; Stumpf, T.; Patzschke, M.; Ikeda-Ohno, A. $[UO_2Cl_2(phen)_2]$, a Simple Uranium(VI) Compound with a Significantly Bent Uranyl Unit (phen=1,10-phenanthroline). *Chem. Eur. J.* **2017**, *23*, 13574–13578.

(56) Carter, K. P.; Kalaj, M.; Kerridge, A.; Ridenour, J. A.; Cahill, C. L. How to Bend the Uranyl Cation via Crystal Engineering. *Inorg. Chem.* **2018**, *57*, 2714–2723.

(57) DIRAC, a relativistic ab initio electronic structure program, Release DIRAC22 (2022), written by H. J. Aa. Jensen, R. Bast, A. S. P. Gomes, T. Saue and L. Visscher et al. (available at http://dx.doi.org/10.5281/zenodo.6010450, see also http://www.diracprogram.org), accessed Sep. 29, 2022.

(58) Saue, T.; Bast, R.; Gomes, A. S. P.; Jensen, H. J. A.; Visscher, L.; Aucar, I. A.; Di Remigio, R.; Dyall, K. G.; Eliav, E.; Fasshauer, E., et al. The DIRAC code for relativistic molecular calculations. *J. Chem. Phys.* **2020**, *152*, 204104.

(59) Stanton, R. E.; Havriliak, S. Kinetic balance: A partial solution to the problem of variational safety in Dirac calculations. *J. Chem. Phys.* **1984**, *81*, 1910–1918.

(60) Visscher, L.; Dyall, K. G. Dirac–Fock atomic electronic structure calculations using different nuclear charge distributions. *At. Data Nucl. Data Tables* **1997**, *67*, 207–224.

(61) Dubillard, S.; Rota, J.-B.; Saue, T.; Faegri, K. Bonding analysis using localized relativistic orbitals: Water, the ultrarelativistic case and the heavy homologues H_2X (X=Te, Po, eka-Po). *J. Chem. Phys.* **2006**, *124*, 154307.

(62) Visscher, L.; Lee, T. J.; Dyall, K. G. Formulation and implementation of a relativistic unrestricted coupled-cluster method including noniterative connected triples. *J. Chem. Phys.* **1996**, *105*, 8769–8776.

(63) Adamo, C.; Barone, V. Toward reliable density functional methods without adjustable parameters: The PBE0 model. *J. Chem. Phys.* **1999**, *110*, 6158–6170.

(64) Ernzerhof, M.; Scuseria, G. E. Assessment of the Perdew–Burke–Ernzerhof exchange-correlation functional. *J. Chem. Phys.* **1999**, *110*, 5029–5036.

(65) Sikkema, J.; Visscher, L.; Saue, T.; Iliaš, M. The molecular mean-field approach for correlated relativistic calculations. *J. Chem. Phys.* **2009**, *131*, 124116.

(66) Dyall, K. G. Relativistic double-zeta, triple-zeta, and quadruple-zeta basis sets for the light elements H–Ar. *Theor. Chem. Acc.* **2016**, *135*, 128.

(67) Dyall, K. G. Relativistic double-zeta, triple-zeta, and quadruple-zeta basis sets for the actinides Ac–Lr. *Theor. Chem. Acc.* **2007**, *117*, 491–500.

(68) Visscher, L. Approximate molecular relativistic Dirac-Coulomb calculations using a simple Coulombic correction. *Theor. Chem. Acc.* **1997**, *98*, 68–70.

(69) Mulliken, R. S. Electronic Population Analysis on LCAO–MO Molecular Wave Functions. I. *J. Chem. Phys.* **1955**, *23*, 1833–1840.

(70) Jensen, F. *Introduction to Computational Chemistry*; Willey-VCH, Weinheim, 2007; p 624.

(71) Knizia, G. Intrinsic Atomic Orbitals: An Unbiased Bridge between Quantum Theory and Chemical Concepts. *J. Chem. Theory Comput.* **2013**, *9*, 4834–4843.

(72) Janak, J. F. Proof that $\partial E/\partial n_i = \epsilon_i$ in density-functional theory. *Phys. Rev. B Condens. Matter* **1978**, *18*, 7165–7168.

(73) Pipek, J.; Mezey, P. G. A fast intrinsic localization procedure applicable for ab initio and semiempirical linear combination of atomic orbital wave functions. *J. Chem. Phys.* **1989**, *90*, 4916–4926.

(74) Herzberg, G. Zum Aufbau der zweiatomigen Moleküle. *Zeitschrift für Physik* **1929**, *57*, 601–630.

(75) Kramida, A.; Yu. Ralchenko,; Reader, J.; and NIST ASD Team, NIST Atomic Spectra Database (ver. 5.9), [Online]. Available: `https://physics.nist.gov/asd` [2017, April 9]. National Institute of Standards and Technology, Gaithersburg, MD., 2021.

(76) Veal, B. W.; Lam, D. J.; Carnall, W. T.; Hoekstra, H. R. X-ray photoemission spectroscopy study of hexavalent uranium compounds. *Phys. Rev. B Condens. Matter* **1975**, *12*, 5651–5663.

(77) Schindler, M.; Hawthorne, F. C.; Freund, M. S.; Burns, P. C. XPS spectra of uranyl minerals and synthetic uranyl compounds. I: The U 4f spectrum. *Geochim. Cosmochim. Acta* **2009**, *73*, 2471–2487.

(78) Pereira, C. C. L.; Michelini, M. d. C.; Marçalo, J.; Gong, Y.; Gibson, J. K. Synthesis and properties of uranium sulfide cations. An evaluation of the stability of thiouranyl, $S{=}U{=}S^{2+}$. *Inorg. Chem.* **2013**, *52*, 14162–14167.

(79) Lucena, A. F.; Bandeira, N. A. G.; Pereira, C. C. L.; Gibson, J. K.; Marçalo, J. Synthesis, structure and bonding of actinide disulphide dications in the gas phase. *Phys. Chem. Chem. Phys.* **2017**, *19*, 10685–10694.

(80) Platts, J. A.; Baker, R. J. A computational investigation of orbital overlap versus energy degeneracy covalency in $[UE_2]^{2+}$ (E = O, S, Se, Te) complexes. *Dalton Trans.* **2020**, *49*, 1077–1088.

(81) Metzler, L. J.; Farmen, C. T.; Fry, A. N.; Seibert, M. P.; Massari, K. A.; Corcovilos, T. A.; van Stipdonk, M. J. Intrinsic reactivity of $[OUCH]^+$: Apparent synthesis of $[OUS]^+$ by reaction with CS_2. *Rapid Commun. Mass Spectrom.* **2022**, *36*, e9260.

(82) Brown, J. L.; Fortier, S.; Wu, G.; Kaltsoyannis, N.; Hayton, T. W. Synthesis and spectroscopic and computational characterization of the chalcogenido-substituted analogues of the uranyl ion, $[OUE]^{2+}$ (E = S, Se). *J. Am. Chem. Soc.* **2013**, *135*, 5352–5355.

(83) Larsson, S.; Pyykkö, P. Relativistically parameterized extended hückel calculations. IX. An iterative version with applications to some xenon, thorium and uranium compounds. *Chem. Phys.* **1986**, *101*, 355–369.

(84) Van Stipdonk, M. J.; Michelini, M. d. C.; Plaviak, A.; Martin, D.; Gibson, J. K. Formation of bare UO_2^{2+} and NUO^+ by fragmentation of gas-phase uranyl-acetonitrile complexes. *J. Phys. Chem. A* **2014**, *118*, 7838–7846.

(85) van Stipdonk, M. J.; Tatosian, I. J.; Iacovino, A. C.; Bubas, A. R.; Metzler, L. J.; Sherman, M. C.; Somogyi, A. Gas-Phase Deconstruction of UO_2^{2+}: Mass Spectrometry Evidence for Generation of $[OU^{VI}CH]^+$ by Collision-Induced Dissociation of $[U^{VI}O_2(C{\equiv}CH)]^+$. *J. Am. Soc. Mass Spectrom.* **2019**, *30*, 796–805.

(86) Van Stipdonk, M. J.; Perez, E. H.; Metzler, L. J.; Bubas, A. R.; Corcovilos, T.; Somogyi, A. Destruction and reconstruction of UO_2^{2+} using gas-phase reactions. *Phys. Chem. Chem. Phys.* **2021**, *23*, 11844–11851.

TOC Graphic

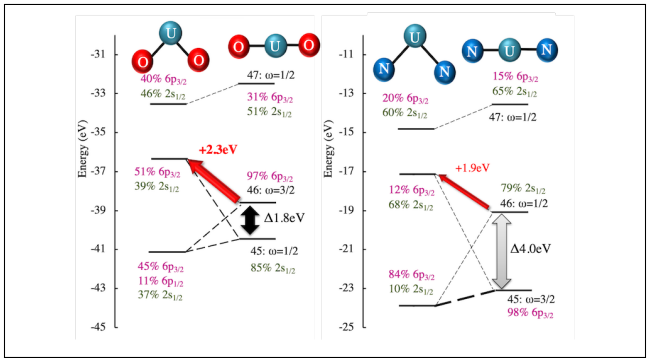
Energy (eV)
-31
-33
-35
-37
-39
-41
-43
-45
40% 6p3/2
46% 2s1/2
47: ω=1/2
31% 6p3/2
51% 2s1/2
+2.3eV
51% 6p3/2
39% 2s1/2
97% 6p3/2
46: ω=3/2
Δ1.8eV
45: ω=1/2
85% 2s1/2
45% 6p3/2
11% 6p1/2
37% 2s1/2
Energy (eV)
-11
-13
-15
-17
-19
-21
-23
-25
20% 6p3/2
60% 2s1/2
15% 6p3/2
65% 2s1/2
47: ω=1/2
+1.9eV
12% 6p3/2
68% 2s1/2
79% 2s1/2
46: ω=1/2
Δ4.0eV
84% 6p3/2
10% 2s1/2
45: ω=3/2
98% 6p3/2